Supporting Information for

Confining FeSe/NiSe heterostructure in *in-situ* formed carbon microspheres for high-efficiency sodium storage

Yu Fei Zheng,[†a] Jie Bai,[†a] Zi Wen,[a] Hong Zhang,*[a] Bei Bei Xiao,*[b] Chun Cheng Yang,*[a] and Qing Jiang[a]

a Key Laboratory of Automobile Materials (Jilin University), Ministry of Education, and School of Materials Science and Engineering, Jilin University, Changchun 130022, China

b School of Energy and Power Engineering, Jiangsu University of Science and Technology, Zhenjiang 212003, China

* Corresponding authors. E-mails: zhanghongjlu@jlu.edu.cn (H. Zhang), xbb420@just.edu.cn (B. B. Xiao), ccyang@jlu.edu.cn (C. C. Yang).
† These authors contributed equally to this work.

Experimental section

Materials synthesis

Synthesis of Fe/Ni-PVP-CA, Fe-PVP-CA, and Ni-PVP-CA: After mixing with 25 mL ethylene glycol (EG) and 25 mL deionized water (DI), 0.4 g polyvinylpyrrolidone (PVP, K30), 2.5 mmol (0.5942 g) $NiCl_2 \cdot 6H_2O$, 2.5 mmol (0.4975 g) $FeCl_2 \cdot 4H_2O$, and 1.4705 g sodium citrate dihydrate ($C_6H_5Na_3O_7 \cdot 2H_2O$, CA) were dissolved in above solution. Subsequently, the solution was transferred to a Teflon-lined sealed autoclave and heated for 12 h at 180 °C. Following cooling of the autoclave to room temperature, Fe/Ni-PVP-CA underwent centrifugation, rinsing with DI and ethanol, and final drying at 80 °C. Fe-PVP-CA (only adding 5 mmol $FeCl_2 \cdot 4H_2O$) and Ni-PVP-CA (only adding 5 mmol $NiCl_2 \cdot 6H_2O$) were synthesized by a similar method.

Synthesis of FeNiSe@C, FeSe@C, and NiSe@C: The Se powder and Fe/Ni-PVP-CA (a mass ratio of 3:1) were placed in two quartz boats, where the Se powder was positioned upstream and Fe/Ni-PVP-CA was positioned downstream in a tube furnace. They were heated at 600 °C (2 °C min^{-1}) for 3 h (95% Ar/5% H_2). NiSe@C (using Ni-PVP-CA) and FeSe@C (using Fe-PVP-CA and annealing at 700 °C) were prepared by the above procedure.

Synthesis of FeNiSe, FeNiSe@C-500, and FeNiSe@C-700: FeNiSe using a similar method to that used for FeNiSe@C, with the exception of adding any carbon source (PVP and $C_6H_5Na_3O_7 \cdot 2H_2O$). FeNiSe@C-500 and FeNiSe@C-700 were prepared by subjecting the Fe/Ni-PVP-CA to annealing at 500 °C and 700 °C, respectively.

Material characterization

The morphologies, microstructures, elemental mappings, and crystal structures were observed using the field emission scanning electron microscopy (FESEM, JSM-7900F, JEOL), transmission electron microscopy (TEM, JEM-2100F, JEOL), and X-ray diffraction (XRD, D/max2500pc, Cu-Kα radiation). The Raman spectra were acquired on a micro-Raman spectrometer (Renishaw). The Brunauer-Emmett-Teller specific surface area and pore structure were measured with ASAP 2020 PLUS HD88. X-ray photoelectron spectroscopy was carried out by Thermo Fisher ESCALAB Xi+. Thermogravimetric analysis (TGA, SDT Q600) was used to investigate the carbon, FeSe, and NiSe content. The Fe and Ni ratio in FeNiSe@C was analyzed by Inductively Coupled Plasma-Optical Emission Spectrometry (ICP-OES, Thermo Scientific).

Electrochemical measurements

CR2025-type coin cells were constructed to measure the Na^+ storage properties of FeNiSe@C, FeSe@C, NiSe@C, FeNiSe, FeNiSe@C-500, and FeNiSe@C-700. The coin cells consisted of the anode (active materials), the counter electrode (metal Na), the separator [glass fiber membrane (Whatman GF/C)], as well as 1 M $NaPF_6$ dissolved in 1,2-dimethoxyethane as the electrolyte. The electrolyte dosage for per coin cell is in the range of 150~200 μL. The slurry was prepared by mixing the active material (70 wt%), Super P (20 wt%), and sodium carboxymethyl cellulose (10 wt%) with DI and applied to the clean copper foil. For each disk with a diameter/area of 12 mm/1.13 cm^2, the mass loading was controlled at 0.6-1.0 mg cm^{-2}. At 2 A g^{-1}, a discharge capacity

(0.35 mAh cm^{-2}) of FeNiSe@C is maintained after 100 cycles (Fig. S20). The anode thickness ranges from 6 to 10 μm. The galvanostatic charge-discharge (GCD), rate capability, and galvanostatic intermittent titration technique (GITT) were conducted on the LAND battery test system (CT2001A) (0.01-3.0 V). The GITT tests were carried out with a pulse current at 0.1 A g^{-1} for 30 min and followed by a relaxation time of 60 min. Cyclic voltammetry curves (CV) and *in-situ* electrochemical impedance spectra (100 kHz-0.1 Hz) were carried out on Ivium-n-Stat. Before conducting the tests for the durability, the cells were activated by cycling at 1.0 A g^{-1} for five cycles. For the sodium ion full cells (1.0-3.4 V), commercial $Na_3V_2(PO_4)_3$ (NVP) and FeNiSe@C were utilized as the cathode and anode, respectively. The N/P ratio (areal capacity of anode/areal capacity of cathode) is about 1. The cathode was fabricated by blending NVP (80 wt%), Super P (10 wt%), and polyvinylidene fluoride (10 wt%) with N-methyl-2-pyrrolidone. The electrolyte and separator are the same as those of the half cells. Before full cell assembling, the FeNiSe@C anode was pre-activated for 5 cycles.

Computational details

All the calculations are performed in the framework of the spin-polarized density functional theory with the projector augmented plane-wave method, as implemented in the Vienna ab initio simulation package.[1] The generalized gradient approximation proposed by Perdew, Burke, and Ernzerhof is selected for the exchange-correlation potential.[2] The long range van der Waals interaction is described by the DFT-D3 approach.[3] The cut-off energy for the plane wave is set to 500 eV. The energy criterion is set to 10^{-5} eV in the iterative solution of the Kohn-Sham equation. A vacuum layer

of 15 Å is added perpendicular to the sheet to avoid artificial interaction between periodic images. The Brillouin zone integration is performed using a 3×1×1 k-mesh. All the structures are relaxed until the residual forces on the atoms have declined to less than 0.05 eV/Å.

Supplementary Figures

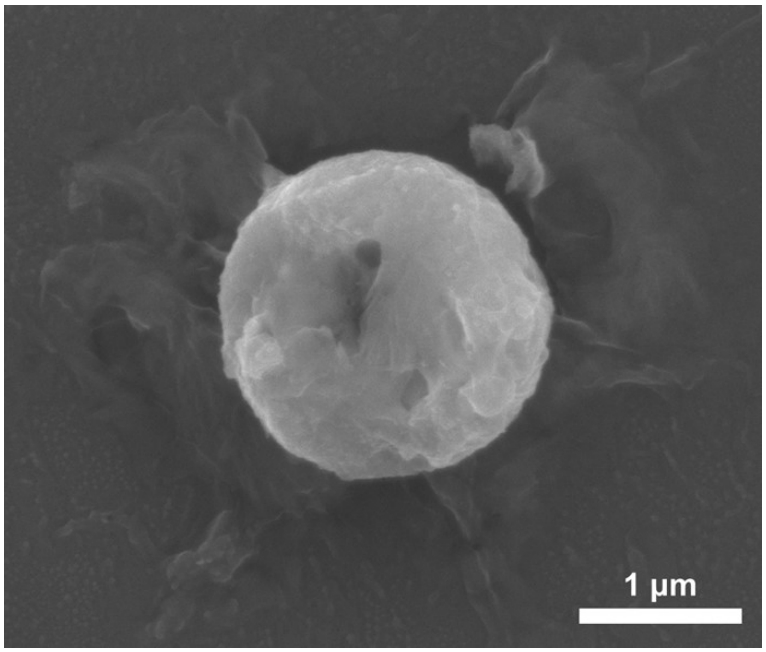

Fig. S1 SEM image of FeNiSe@C.

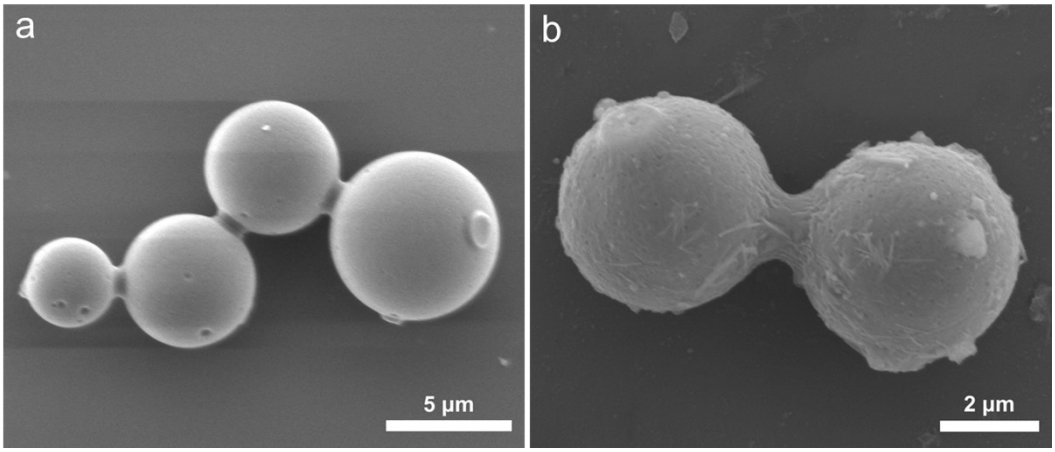

Fig. S2 SEM images of (a) Fe-PVP-CA and (b) FeSe@C.

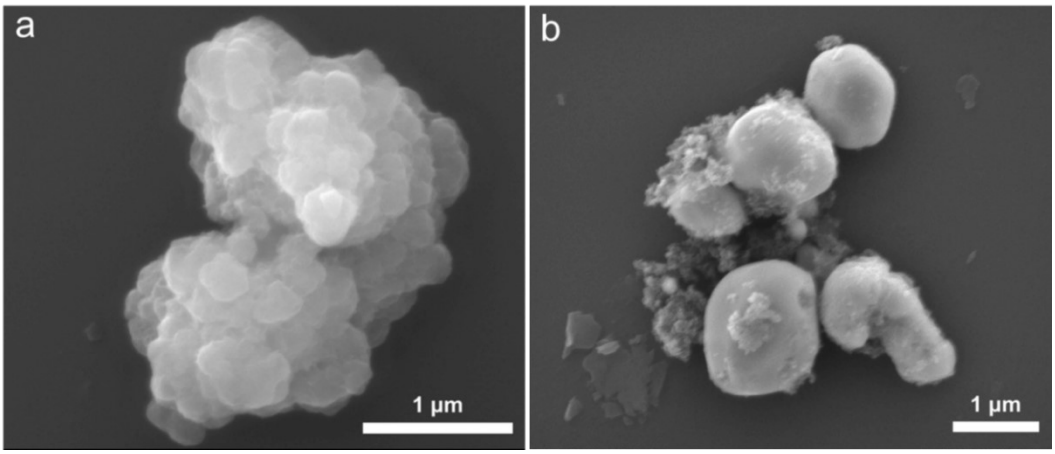

Fig. S3 SEM images of (a) Ni-PVP-CA and (b) NiSe@C.

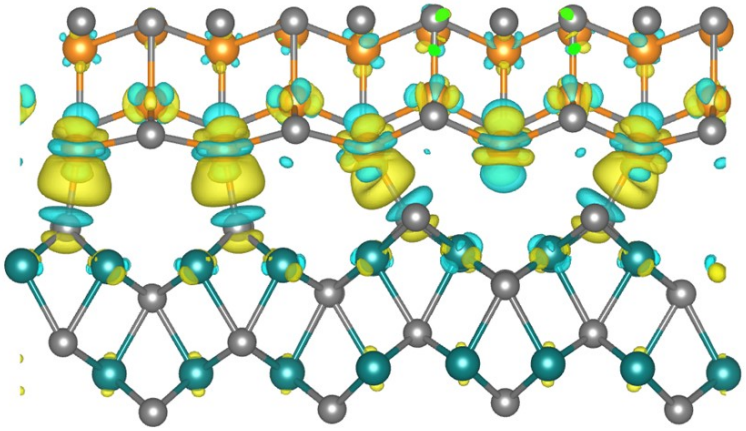

Fig. S4 Charge density difference for FeSe/NiSe heterostructure, where yellow and blue regions correspond to charge aggregation and depletion, respectively.

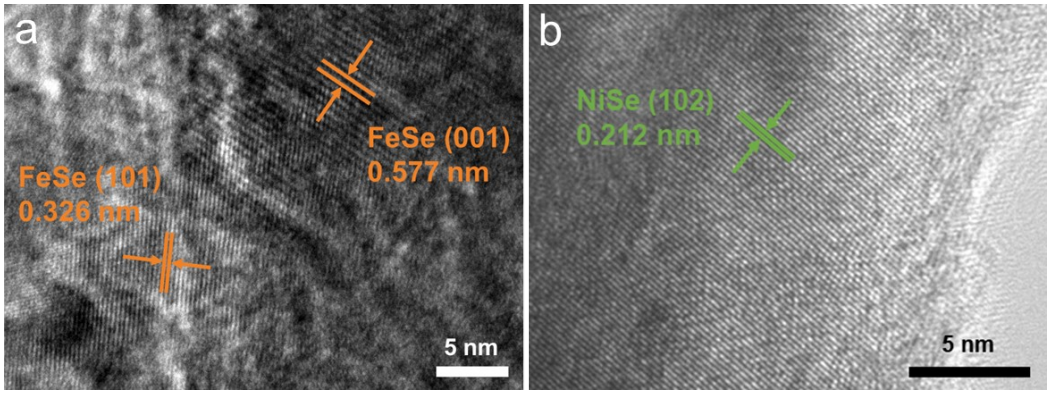

Fig. S5 (a, b) High-resolution TEM images of FeNiSe@C.

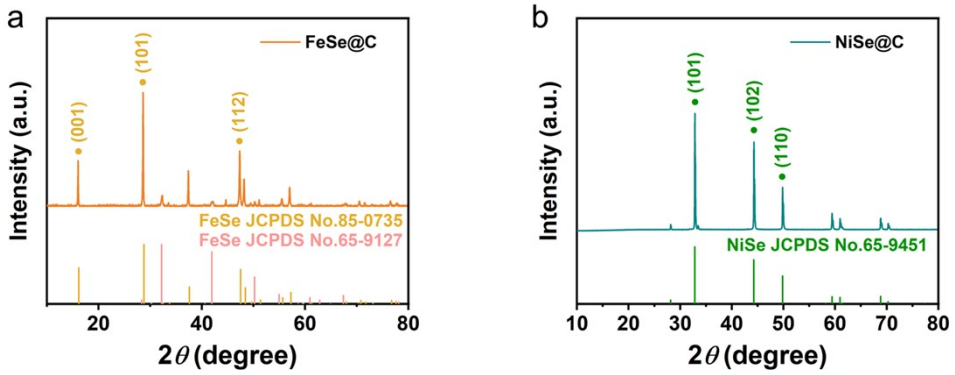

Fig. S6 XRD patterns of (a) FeSe@C and (b) NiSe@C.

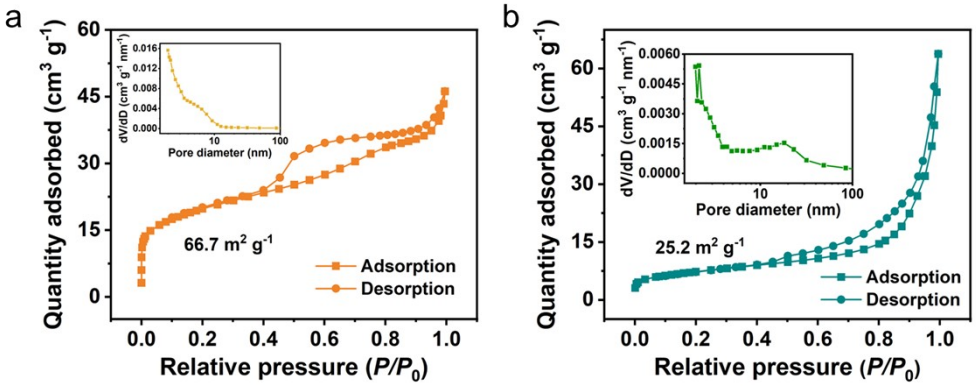

Fig. S7 Nitrogen adsorption-desorption isothermal curves and pore size distribution curves of (a) FeSe@C and (b) NiSe@C.

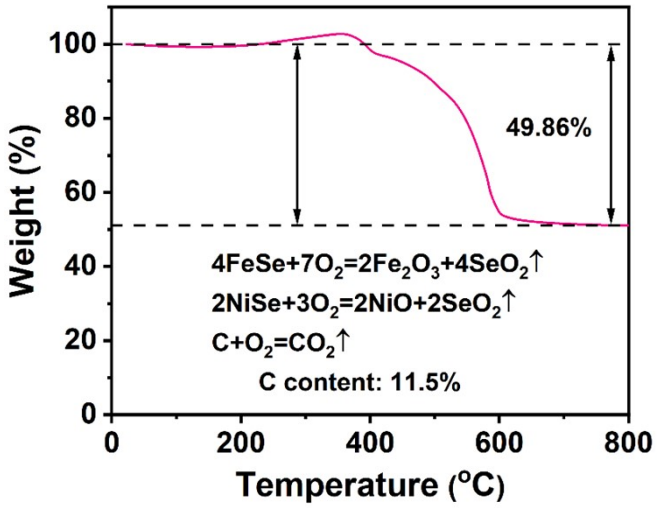

Fig. S8 TGA curve of FeNiSe@C.

The weight ratio of Fe: Ni is 1 for FeNiSe@C by ICP-OES (Table S1).

We assume the weight percentage of NiSe is y, so the weight percentage of FeSe is calculated to be:

FeSe (wt%):

$$\frac{\text{weight of NiSe} \times 0.85 \times \text{molecular weight of Ni}}{\text{molecular weight of NiSe}} \times \frac{\text{molecular weight of FeSe}}{\text{molecular weight of Fe}} = \frac{y \times 59}{138} \times \frac{135}{56} = 1.03y$$

Fe_2O_3 (wt%):

$$\frac{2 \times \text{molecular weight of } Fe_2O_3 \times \text{weight of FeSe}}{4 \times \text{molecular weight of FeSe}} = \frac{2 \times 160 \times 1.03y}{4 \times 135} = 0.61y$$

NiO (wt%):

$$\frac{2 \times \text{molecular weight of NiO} \times \text{weight of NiSe}}{2 \times \text{molecular weight of NiSe}} = \frac{2 \times 75 \times y}{4 \times 138} = 0.54y$$

$$\frac{2 \times \text{molecular weight of } Fe_2O_3 \times \text{weight of FeSe}}{4 \times \text{molecular weight of FeSe}} + \frac{2 \times \text{molecular weight of NiO} \times \text{weight of NiSe}}{2 \times \text{molecular weight of NiSe}}$$

$= 1 - 49.86\%$

$$\frac{2 \times 160 \times 1.03y}{4 \times 135} + \frac{2 \times 75 \times y}{4 \times 138} = 50.14\%$$

$y = 43.6\%$

$1.03y = 44.9\%$

Thus, the weight percentages of NiSe and FeSe are 43.6% and 44.9%, respectively.

And the weight percentage of carbon is 1-43.6%-44.9% = 11.5%.

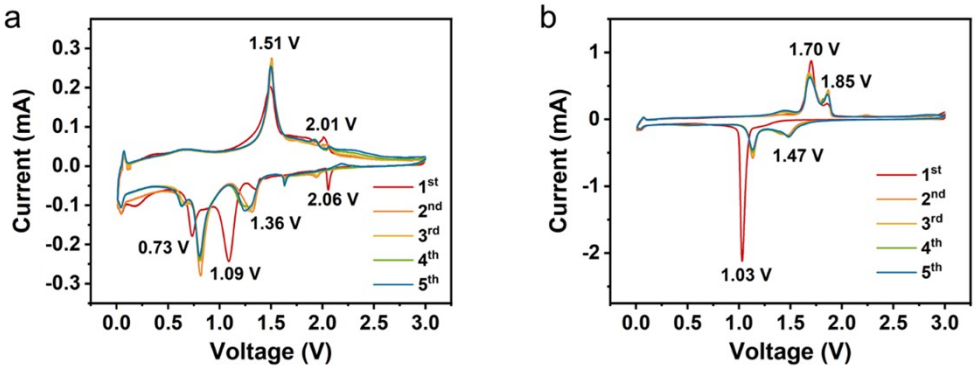

Fig. S9 CV curves of (a) FeSe@C and (b) NiSe@C.

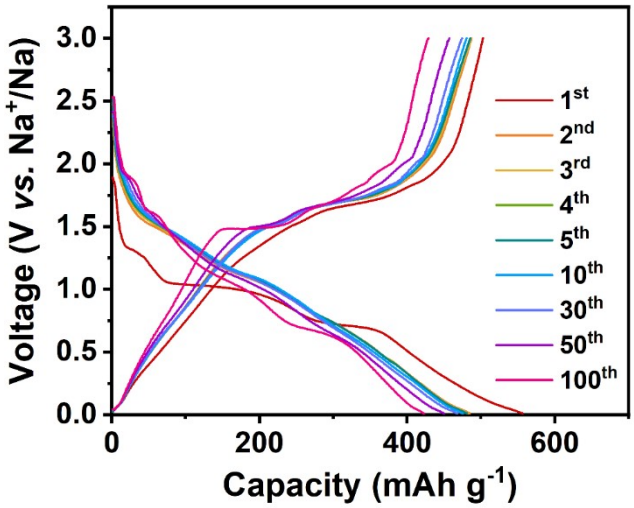

Fig. S10 GCD profiles at 2.0 A g^{-1}.

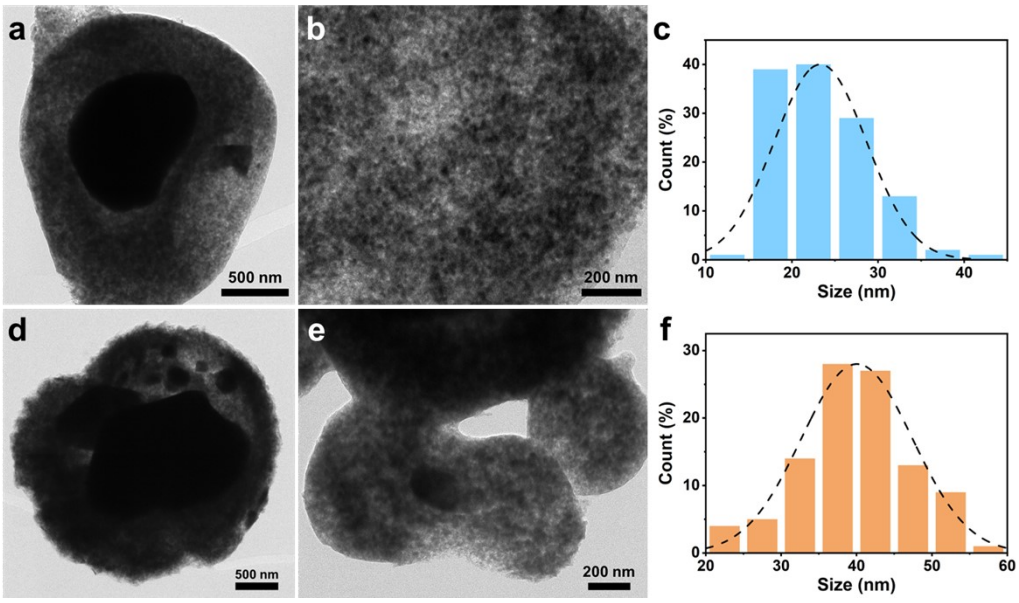

Fig. S11 (a, b) TEM images of FeNiSe@C-500 and (c) the corresponding size distribution of the FeNiSe particles. (d, e) TEM images of FeNiSe@C-700 and (f) the corresponding size distribution of the FeNiSe particles.

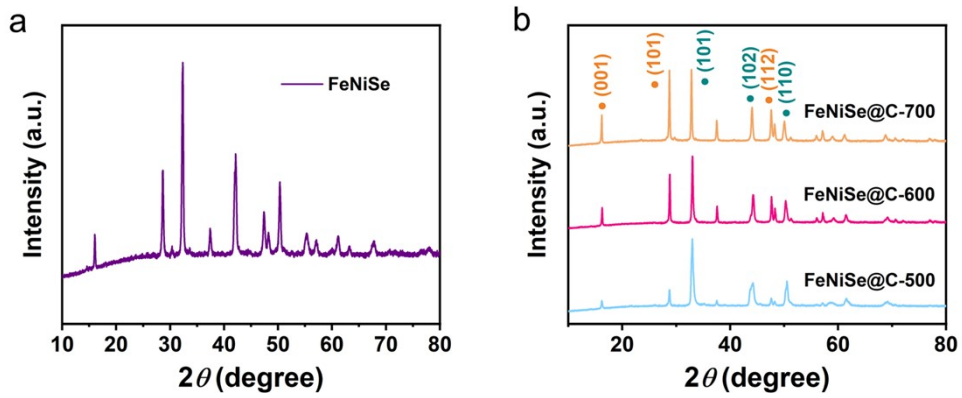

Fig. S12 (a) XRD pattern of FeNiSe. (b) XRD patterns of FeNiSe@C-500, FeNiSe@C-600, and FeNiSe@C-700.

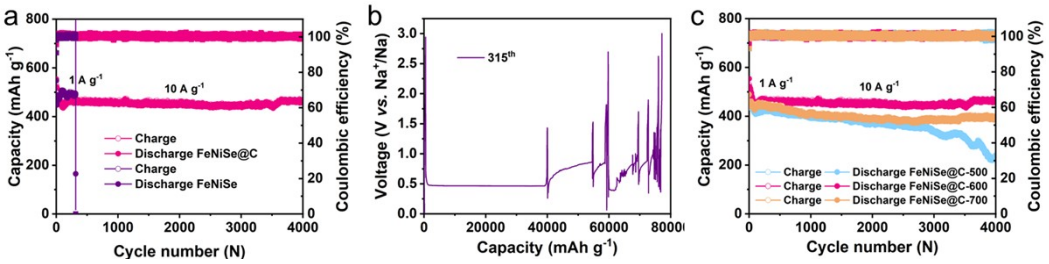

Fig. S13 (a) Long-term cycling performance of FeNiSe@C and FeNiSe at 10 A g^{-1}. (b) GCD profile of FeNiSe for the 315th cycle at 10 A g^{-1}. (c) Long-term cycling performance of FeNiSe@C-500, FeNiSe@C-600, and FeNiSe@C-700 at 10 A g^{-1}.

The N-doped carbon layer can act as a conducting medium to facilitate Na^+/ion diffusion and reinforce the structural stability.[4,5] Fig. S12a demonstrates the successful synthesis of the FeNiSe. The GITT (Fig. S17a, b) and cycling performance (Fig. S13a, b) profiles of FeNiSe@C with N-doped carbon and FeNiSe without them confirm that FeNiSe@C possesses excellent Na^+ diffusion kinetics and long-term cyclability over 4000 cycles, whereas FeNiSe displays a smaller average D_{Na+} (2.08×10^{-12} and 2.23×10^{-12} cm^2 s^{-1}) and experiences an "under-voltage failure" at the 315th cycle, leading to a dead battery.[6] Thus, the N-doped carbon layer ensures the stable operation of the battery.

Reducing the particle size facilitates Na^+ ion transport by shortening the diffusion pathway.[7] As shown in Fig. S11a, b, d, and e, FeNiSe@C-500 and FeNiSe@C-700 all show a spherical morphology. Notably, the average particle diameter of FeNiSe nanoparticles exhibits a temperature-dependent increase across these three samples (Fig. S11c, f). The average sizes of FeNiSe nanoparticles are approximately 23 nm (500 °C), 35 nm (600 °C), and 40 nm (700 °C), respectively. Moreover, when the annealing

temperature rises from 500 to 700 °C, the intensity of the X-ray diffraction (XRD) patterns (Fig. S12b) gradually strengthens, indicating that the crystallinity of the samples increases with increasing annealing temperature. As reported in previous literature, high crystallinity implies better stability of the materials and provides fast Na^+ conduction channels.[8,9] However, excessive crystallinity means a low content of defects, which also leads to a decrease in active sites for Na^+ storage, resulting in the capacity loss.[8] The cycling performance (Fig. S13c) and GITT (Fig. S17c, d) profiles of FeNiSe@C synthesized at different calcination temperatures indicate FeNiSe@C-600 with the moderate particle size and crystallinity displays the best cycling durability over 4000 cycles and Na^+ diffusion kinetics compared with FeNiSe@C-500 (48.2% and 1.13×10^{-12}/9.23×10^{-13} cm^2 s^{-1}) and FeNiSe@C-700 (79.1% and 1.95×10^{-12} and 1.37×10^{-12} cm^2 s^{-1}). The smaller particle size for the shortened Na^+ diffusion path, along with the heterointerface and carbon coating effects, synergistically improves the electrochemical kinetics.

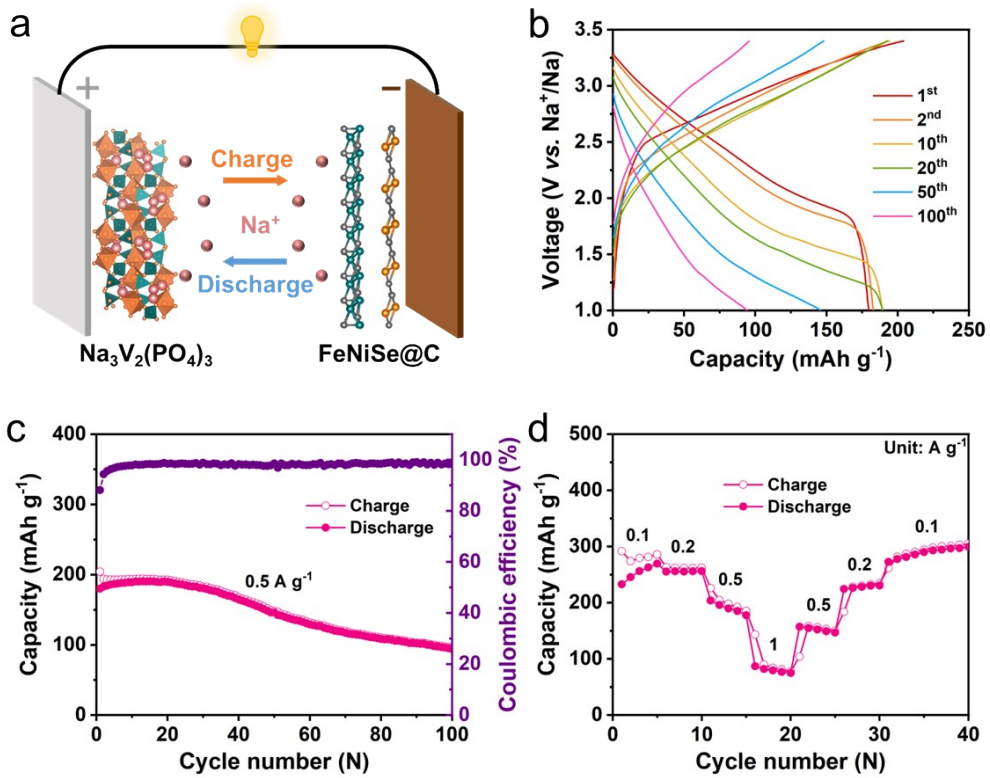

Fig. S14 (a) The schematic diagram of the FeNiSe@C//NVP full cell. (b) GCD profiles at 0.5 A g^{-1}, (c) Cycling performance at 0.5 A g^{-1}, and (d) Rate capability of the FeNiSe@C//NVP full cell at various current densities.

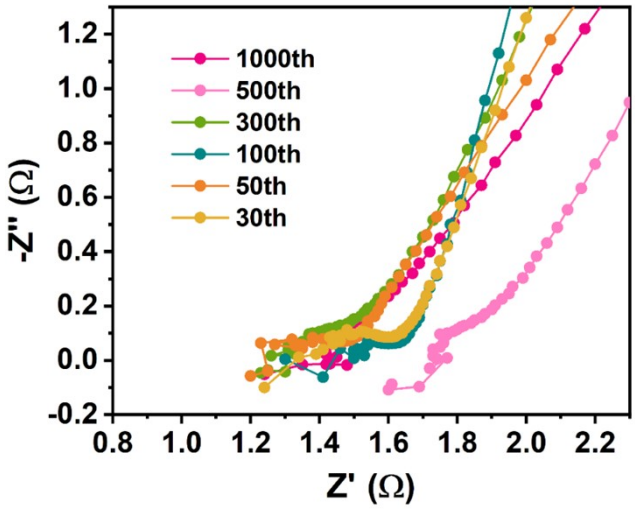

Fig. S15 Nyquist plots of FeNiSe@C at different cycles.

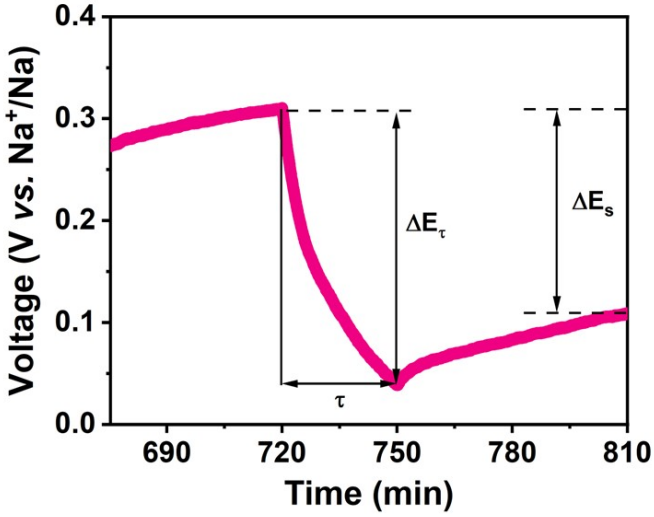

Fig. S16 Detailed voltage response curves of FeNiSe@C during a single constant current pulse with respect to time.

The Na^+ diffusion coefficient (D_{Na+}) can be calculated through the following equation:[10]

$$D_{Na^+} = \frac{4}{\pi\tau}\left(\frac{mV_m}{MA}\right)^2\left(\frac{\Delta E_s}{\Delta E_\tau}\right)^2 \quad \text{(S1)}$$

where m, $V_{m,}$ and M denote the mass, molar volume, and molar mass, respectively. τ refers to the duration of the pulse. A denotes the electrode area. ΔE_s is the potential change between two steady states caused by the current pulse, and ΔE_τ is the transient potential change caused by the constant charging/discharging process.

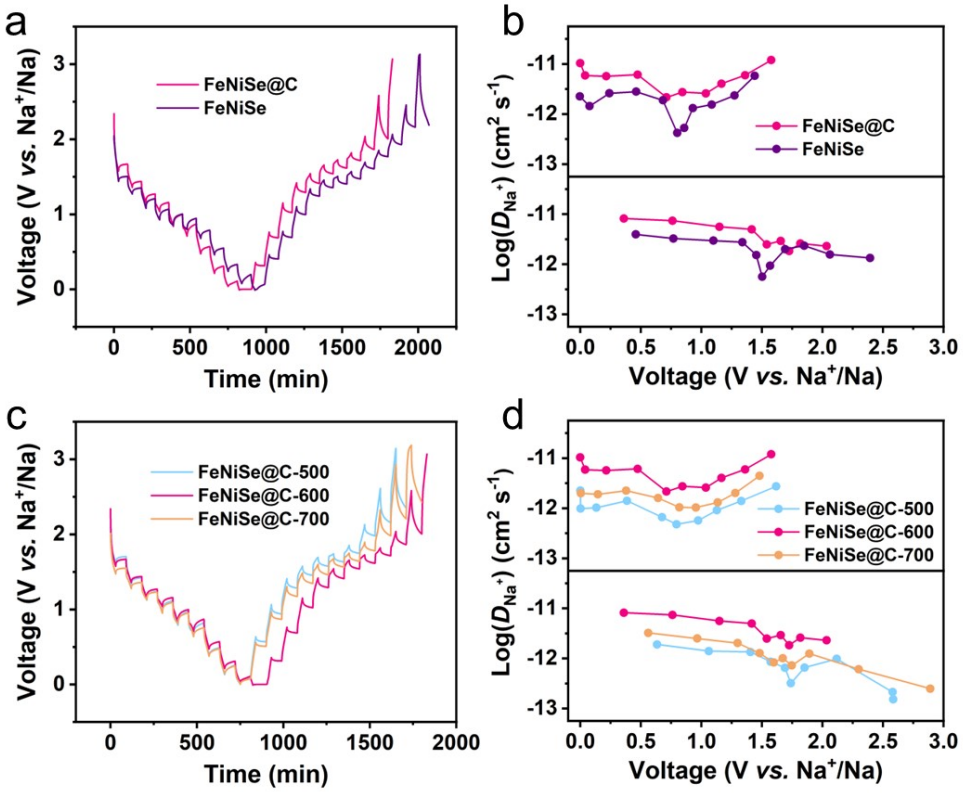

Fig. S17 (a) GITT voltage profiles and (b) the corresponding D_{Na+} during the discharge and charge processes of FeNiSe@C and FeNiSe. (c) GITT voltage profiles and (d) the corresponding D_{Na+} during the discharge and charge processes of FeNiSe@C-500, FeNiSe@C-600, and FeNiSe@C-700.

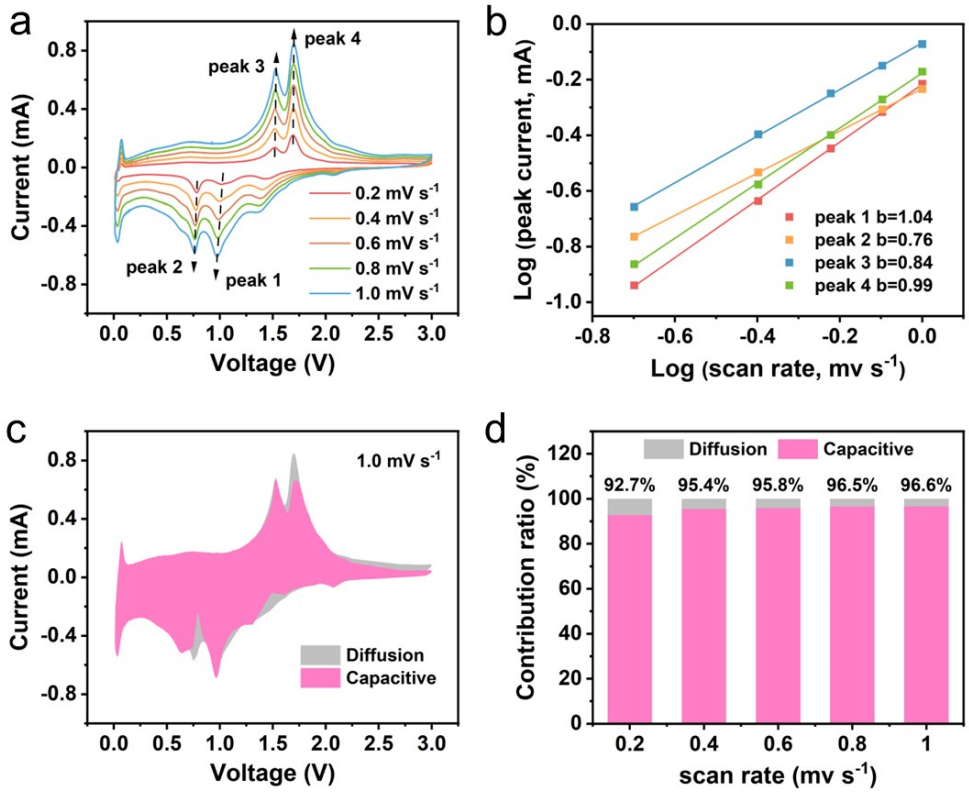

Fig. S18 (a) CV curves of FeNiSe@C at different scan rates. (b) b values determined by correlation of log(i)-log(v). (c) Normalized contribution ratio for FeNiSe@C at 1.0 mV s^{-1}. (d) Capacitive and diffusion-controlled contribution ratios of FeNiSe@C.

To evaluate the diffusion and pseudocapacitive contributions, we performed CV tests of FeNiSe@C at different scan rates (Fig. S18a). The relationship of the scanning rate (v) and peak current (i) can be described as:[11]

$$i = av^b \tag{S2}$$

where both a and b are variables. The b value of 0.5/1.0 is characteristic of a diffusion/capacitive-dominated process. As depicted in Fig. S18b, the b values are 1.04 (peak 1), 0.76 (peak 2), 0.84 (peak 3), and 0.99 (peak 4), respectively, suggesting that the electrochemical reaction process is dominated by both diffusive and

pseudocapacitive behaviors. The quantitative contributions of capacitive (k_1v) and diffusion process ($k_2v^{1/2}$) in FeNiSe@C can be calculated based on the following equation:[12]

$$i(\mathrm{V}) = k_1v + k_2v^{1/2} \quad \text{(S3)}$$

With increasing the scan rate, the proportion of the capacitive contribution gradually increases from 92.7% to 96.6% (Fig. S18c, d). This reveals that the capacitive behavior is the dominant charge storage mechanism.

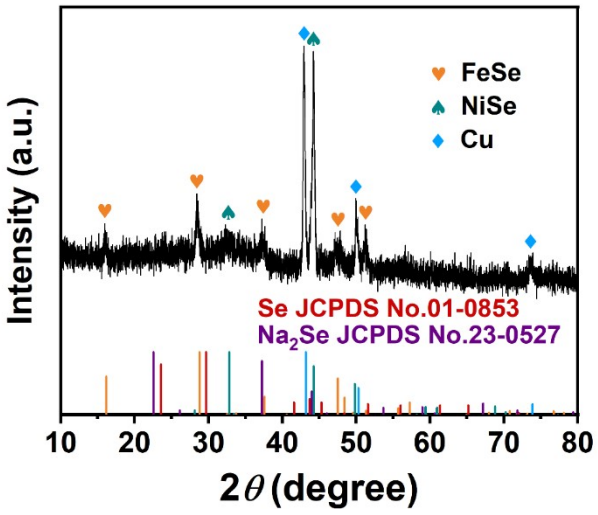

Fig. S19 *Ex-situ* XRD pattern of the FeNiSe@C anode after being charged to 3.00 V.

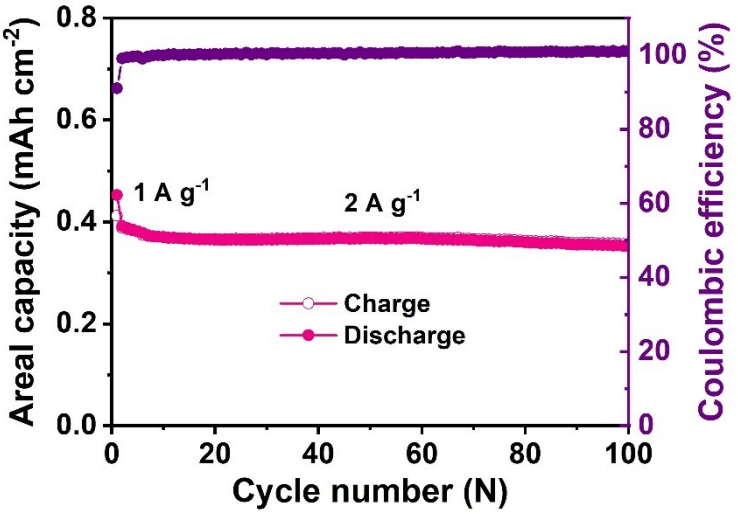

Fig. S20 Cycling performance of FeNiSe@C at 2 A g^{-1} with a mass loading of 0.88 mg cm^{-2}.

Table S1 The ICP-OES analysis results of FeNiSe@C.

Elements	Content (mg/L)	Content (mol/L)	Mole Ration (Fe:Ni)
Fe	1.113	1.401	1:1
Ni	1.177	1.486	

Supplementary References

1 G. Kresse and D. Joubert, *Phys. Rev. B*, 1999, **59**, 1758-177.

2 J. P. Perdew, K. Burke and M. Ernzerhof, *Phys. Rev. Lett.*, 1996, **77**, 3865-3868.

3 S. Grimme, J. Antony, S. Ehrlich and H. Krieg, *J. Chem. Phys*, 2010, **132**, 154104.

4 J. Wang, B. Wang, H. Sun, G. Wang, J. Bai and H. Wang, *Energy Storage Mater.*, 2022, **46**, 394-405.

5 Yang, H. Fu, Y. Duan, M. Wang, M. X. Tran, J. K. Lee, W. Yang and G. Liu, *Energy Environ. Mater.*, 2023, **6**, e12380.

6 J. Xu, M. Zhang, F. Cao, X. Chen, X. Chen, J. Chen, Y. Zhang, J. Zhang and W. Kang, *J. Power Sources*, 2023, **573**, 233132.

7 P. Ge, H. Hou, S. Li, L. Yang and X. Ji, *Adv. Funct. Mater.*, 2018, **28**, 1801765.

8 Y. Dong, Y. Xu, W. Li, Q. Fu, M. Wu, E. Manske, J. Kröger and Y. Lei, *Small*, 2019, **15**, 1900497.

9 J. Yin, P. Hai, Y. Gao, Z. Gan, C. Wu, Y. Cheng and X. Xu, *Nano Res.*, 2023, **16**, 4941-4949.

10 X. He, Z. Zhao, X. Yang, X. Liu, M. Yang, L. He, J. Zhu, Y. Wang, H. Mi, L. Zhang, C. He, D. Ma and P. Zhang, *ACS Nano*, 2025, **19**, 30243-30253.

11 Y. Shi, P. Mei, T. He, C. Deng, H. Ba, J. Hu and S. Huang, *Chem. Eng. J.*, 2024, **497**, 155682.

12 T. Feng, F. Wang, Z. Sun, F. Guo, Y. Xiong, F. Ren, C. Tang, J. Li, H. K. Liu and S. X. Dou, *Angew. Chem. Int. Ed.*, 2025, **64**, e202420504.